Structural basis for antibiotic resistance mediated by the *Bacillus subtilis* ABCF ATPase VmlR

Caillan Crowe-McAuliffe[a], Michael Graf[a], Paul Huter[a], Hiraku Takada[b,c], Maha Abdelshahid[a], Jiří Nováček[d], Victoriia Murina[b], Gemma C. Atkinson[b], Vasili Hauryliuk (Василий Гаврилюк)[b,c,e], and Daniel N. Wilson[a,1]

[a]Institute for Biochemistry and Molecular Biology, University of Hamburg, 20146 Hamburg, Germany; [b]Department of Molecular Biology, Umeå University, 90187 Umeå, Sweden; [c]Laboratory for Molecular Infection Medicine Sweden, Umeå University, 90187 Umeå, Sweden; [d]Central European Institute of Technology, Masaryk University, 62500 Brno, Czech Republic; and [e]Institute of Technology, University of Tartu, 50411 Tartu, Estonia

Edited by Peter B. Moore, Yale University, New Haven, CT, and approved July 23, 2018 (received for review May 17, 2018)

Many Gram-positive pathogenic bacteria employ ribosomal protection proteins (RPPs) to confer resistance to clinically important antibiotics. In *Bacillus subtilis*, the RPP VmlR confers resistance to lincomycin (Lnc) and the streptogramin A (S_A) antibiotic virginiamycin M (VgM). VmlR is an ATP-binding cassette (ABC) protein of the F type, which, like other antibiotic resistance (ARE) ABCF proteins, is thought to bind to antibiotic-stalled ribosomes and promote dissociation of the drug from its binding site. To investigate the molecular mechanism by which VmlR confers antibiotic resistance, we have determined a cryo-electron microscopy (cryo-EM) structure of an ATPase-deficient *B. subtilis* VmlR-EQ_2 mutant in complex with a *B. subtilis* ErmDL-stalled ribosomal complex (SRC). The structure reveals that VmlR binds within the E site of the ribosome, with the antibiotic resistance domain (ARD) reaching into the peptidyltransferase center (PTC) of the ribosome and a C-terminal extension (CTE) making contact with the small subunit (SSU). To access the PTC, VmlR induces a conformational change in the P-site tRNA, shifting the acceptor arm out of the PTC and relocating the CCA end of the P-site tRNA toward the A site. Together with microbiological analyses, our study indicates that VmlR allosterically dissociates the drug from its ribosomal binding site and exhibits specificity to dislodge VgM, Lnc, and the pleuromutilin tiamulin (Tia), but not chloramphenicol (Cam), linezolid (Lnz), nor the macrolide erythromycin (Ery).

ABC ATPase | cryo-EM | ribosome | antibiotic resistance | VmlR

The ribosome is one of the major targets in the cell for antibiotics, including many clinically important antibiotic classes, for example the streptogramins, lincosamides, pleuromutilins, and macrolides (reviewed in refs. 1 and 2). However, the ever-increasing emergence of multidrug resistant bacteria is rendering our current antibiotic arsenal obsolete. Therefore, it is important to understand the mechanisms that bacteria employ to obtain antibiotic resistance to develop improved antimicrobial agents to overcome these mechanisms. Two important antibiotic resistance strategies employed by bacteria include antibiotic efflux and ribosome protection, both of which can be mediated by members of the large family of ATP-binding cassette (ABC) proteins. ABC proteins involved in drug efflux include membrane-bound transporters that use energy to pump the antibiotic out of the cell. By contrast, ABC proteins of the subclass F (ABCF) do not contain transmembrane domains to anchor them to the membrane and instead confer resistance by binding to the ribosome and chasing the antibiotic from its binding site (reviewed in ref. 3).

Antibiotic resistance (ARE) ABCF proteins are widespread in Gram-positive bacteria but also found in some Gram-negative bacteria (3, 4). ARE-ABCF proteins can be chromosomally and/or plasmid-encoded and are found in many clinically relevant pathogenic bacteria, including *Staphylococcus aureus*, *Enterococcus faecalis*, *Listeria monocytogenes*, and *Escherichia coli* (3, 4). To date, all ARE-ABCF proteins confer resistance to antibiotics that bind to the large ribosomal subunit (LSU), either at the peptidyl-transferase center (PTC) or adjacent to the PTC in the ribosomal exit tunnel. ARE-ABCF proteins can be divided into distinct classes on the basis of their resistance profiles (3, 4). For example, the Vga/Lsa/Sal/Vml class confers resistance to streptogramin A (S_A) antibiotics, lincosamides, and sometimes pleuromutilins, whereas the Msr class confers resistance to streptogramin B (S_B) antibiotics, macrolides, and sometimes ketolides. In *Enterococci*, the ARE-ABCF OptrA has been reported to confer resistance to oxazolidinones and chloramphenicols (5). Several studies have demonstrated that ARE-ABCFs are RPPs that confer resistance by displacing the drug from its binding site on the ribosome (6, 7), analogous to the displacement of tetracycline from the ribosome mediated by the RPPs TetM/TetO (8).

ARE-ABCF proteins comprise two ABC nucleotide-binding domains (NBD1 and NBD2) that are separated by a helical linker and, depending on the species, may have an additional "Arm" subdomain inserted within NBD1 as well as a C-terminal extension (CTE) (4). The ATPase activity of ARE-ABCF proteins is essential for their function since mutations of the catalytic glutamate in NBD1 or NBD2 lead to a loss of the ability of VgaA to confer resistance to VgM (6, 9). Consistently, the inhibition of ribosomal transpeptidation (transfer of fMet from the P-site tRNA to puromycin) that results from the presence of Lnc

Significance

The recent increase in multidrug-resistant pathogenic bacteria is limiting the utility of our current arsenal of clinically important antibiotics. The development of improved antibiotics would therefore benefit from a better understanding of the current resistance mechanisms employed by bacteria. Many Gram-positive bacteria, including pathogenic *Staphylococcus aureus* and *Enterococcus faecalis*, utilize ribosome protection proteins to confer resistance to medically relevant antibiotics, such as streptogramins A, lincosamides, and pleuromutilins. We have employed cryo-electron microscopy to reveal the structural basis for how the *Bacillus subtilis* VmlR protein binds to the ribosome to confer resistance to the streptogramin A antibiotic virginiamycin M, the lincosamide lincomycin, and the pleuromutilin tiamulin.

Author contributions: G.C.A., V.H., and D.N.W. designed research; C.C.-M., H.T., J.N., and G.C.A. performed research; M.A. and V.M. contributed new reagents/analytic tools; C.C.-M., M.G., P.H., H.T., V.H., and D.N.W. analyzed data; and C.C.-M. and D.N.W. wrote the paper.

The authors declare no conflict of interest.

This article is a PNAS Direct Submission.

Data deposition: The atomic coordinates have been deposited in the Protein Data Bank, www.wwpdb.org (PDB ID codes 6HA1 and 6HA8). The cryo-EM maps have been deposited in the Electron Microscopy Data Bank (EMDB ID codes EMD-0176 and EMD-0177).

[1]To whom correspondence should be addressed. Email: daniel.wilson@chemie.uni-hamburg.de.

This article contains supporting information online at www.pnas.org/lookup/suppl/doi:10.1073/pnas.1808535115/-/DCSupplemental.

Published online August 20, 2018.

is relieved by VgaA, but not the catalytically inactive VgaA-EQ$_2$ mutant (4). Similarly, transpeptidation was restored by VgaA in the presence of ATP, but not ADP or nonhydrolysable ATP analogs (4).

ARE-ABCFs are closely related to energy-dependent translational throttle A (EttA), an ABCF protein that binds within the ribosomal E site to regulate translation in response to energy levels in the cell (10, 11). A recent cryo-electron microscopy (cryo-EM) structure of the *Pseudomonas aeruginosa* ARE-ABCF MsrE bound to the *Thermus thermophilus* 70S ribosome revealed that MsrE, like EttA, binds in the E site and has an extended interdomain linker that reaches toward the PTC of the ribosome (7). Large variations in sequence and length are observed within the interdomain linker between different classes of ARE-ABCFs (*SI Appendix*, Fig. S1), and mutations within a loop at the tip of the interdomain linker can alter the antibiotic specificity of the ARE-ABCF proteins (6, 7, 12, 13). Furthermore, VgaA variants where the interdomain linker is truncated cannot restore the ribosomal transpeptidation in the presence of lincomycin (4). While the MsrE-70S structure provides insight into how the Msr class confers resistance to macrolide antibiotics (7), structural insight into how the Vga/Lsa/Sal/Vml class confers resistance to PTC-targeting antibiotics has been lacking.

Here, we have determined a cryo-EM structure of *Bacillus subtilis* VmlR bound to a stalled ribosome complex (SRC) at 3.5-Å resolution, revealing that VmlR, like EttA and MsrE, binds within the E site of the ribosome. The interdomain linker of VmlR accesses the PTC of the ribosome by inducing a noncanonical conformation of the P-site tRNA where the acceptor arm is disengaged from the PTC and the CCA end is shifted toward the A site. While the interdomain linker of VmlR directly encroaches the binding site of PTC-targeting antibiotics, we observe specificity in the VmlR resistance profile, such that VmlR confers resistance to VgM, Lnc, and Tia, but not to Cam, Lnz, or Ery. We also identify a VmlR-F237A variant that exhibits altered specificity, conferring resistance to Lnc and Tia, but not to VgM. Our combined structural and mutagenesis analyses suggest that VmlR dislodges VgM, Lnc, and Tia using an indirect allosteric, rather than a direct steric, mechanism of action.

Results

Generation of a *B. subtilis* VmlR–70S Ribosome Complex. Initially, we in vitro-reconstituted complexes between wild-type VmlR (previously called ExpZ) and tight-coupled *B. subtilis* 70S ribosomes in the presence of the nonhydrolysable ATP analog ADPNP. Despite observing binding in pelleting assays, no density for VmlR was observed in low-resolution cryo-EM reconstructions, suggesting that the VmlR–ribosome interaction was not stable. A previous study employed an ATPase-deficient form of EttA (EttA-EQ$_2$) to trap and visualize the factor in the ATP form on the ribosome using cryo-EM (11). Therefore, we generated an equivalent ATPase-deficient VmlR-EQ$_2$ variant where Glu129 in NBD1 and Glu432 in NBD2 were mutated to Gln129 and Gln432, respectively. A low-resolution cryo-EM reconstruction of the VmlR–EQ$_2$–70S complex revealed density for VmlR in the E site of the 70S ribosomes bearing a tRNA in the P site. Unfortunately, this represented a small percentage of the population, as the P-site tRNAs were only present as contaminants that remained bound to the tight-coupled ribosomes despite the purification process. To increase the ribosomal occupancy of the P-site tRNAs, and thus promote binding of VmlR, we replaced 70S ribosomes with stalled ribosome complexes (SRCs), as used previously to visualize RelA (14) and TetM (15) on the ribosome. To generate the SRCs, translation of an ErmDL stalling peptide in the presence of the ketolide telithromycin was carried out, leading to ribosomes stalled with a short seven-amino acid peptidyl-tRNA decoding the seventh codon of the mRNA (16). In contrast to our previous studies, we performed translation in the *E. coli* PURE system using *B. subtilis* rather than *E. coli* 70S ribosomes (17), thus enabling a homogeneous *B. subtilis* VmlR-EQ$_2$-SRC to be generated. Since VmlR does not confer resistance to the macrolide class of antibiotics (18), we rationalized that using the ErmDL-SRC may also contribute to trapping VmlR on the ribosome. We did not attempt to generate Lnc or VgM SRCs as substrates for VmlR binding, since our past experience in forming TetM-SRC revealed that the presence of the drug (in this case, tetracycline) only generated additional sample heterogeneity due to competition for binding between TetM and tetracycline (19).

Cryo-EM Structure of a *B. subtilis* VmlR-EQ$_2$-SRC. Cryo-EM data for the *B. subtilis* VmlR-EQ$_2$-SRC was collected on a Titan Krios transmission electron microscope (TEM) with a Falcon III direct electron detector (DED) and processed with RELION 2.1 (20). After 2D classification, a total of 159,722 ribosomal particles were sorted into two major populations, both of which contained a P-site tRNA but differed with respect to the presence (18–21%, 28,972–33,392) or absence (43%, 68,652 particles) of VmlR-EQ$_2$ (Fig. 1 and *SI Appendix*, Fig. S2*A*). The cryo-EM maps of the VmlR-EQ$_2$-SRC (Fig. 1*A*) and P-tRNA-SRC could be refined to yield final average resolutions of 3.5 Å and 3.1 Å, respectively (*SI Appendix*, Fig. S2 *B–D*). Molecular models for the *B. subtilis* 70S ribosome were based on a previous model of a *B. subtilis* MifM-SRC (21), which could be improved to include side chains for the proteins of the SSU due to the better resolution (*SI Appendix*, Table S1). The VmlR model was initially based on a homology model generated using the crystal structure of EttA (10) as a template (Fig. 1*B*). The density for the C-terminal extension (CTE) that is absent in EttA and MsrE was modeled as two α-helices connected by a short linker to the NBD2 (Fig. 1*B*), which is consistent with secondary structure predictions; however, the quality of the density map only permitted the backbone to be traced. By contrast, the interdomain linker between NBD1 and NBD2, which we refer to as the antibiotic resistance domain (ARD), was well-resolved and could be modeled de novo (*SI Appendix*, Fig. S2*E*), presumably because the ARD is sandwiched between the 23S rRNA of the LSU and the acceptor arm of the P-site tRNA (Fig. 1*A*). Clear density was observed for two molecules of ATP bound within the active sites formed by NBD1 and NBD2 (Fig. 1*C*), in agreement with the ability of the VmlR-EQ$_2$ to bind, but not hydrolyze, ATP. Consistently, previous studies have shown that EQ mutations in either NBD lead to a loss in the ability of VgaA to confer resistance to VgM (9). NBD1 and NBD2 of VmlR-EQ$_2$ adopt a closed conformation on the ribosome, similar to that observed for the ABC multidrug resistance protein 1 (MRP1) (22) as well as the modeled ATP conformation of EttA (10, 11), but distinct from the open conformation observed for the free state of ABCE1 (23) (*SI Appendix*, Fig. S3 *A–C*).

Binding Site of VmlR on the 70S Ribosome. VmlR binds within the E site of the 70S ribosome (Fig. 1*A*), analogously to EttA (11) (*SI Appendix*, Fig. S3 *D–F*). The NBD1 of VmlR directly contacts and stabilizes an open conformation of the L1 stalk (Fig. 2*A*), which is similar but distinct from that observed in the presence of EttA due to the EttA "Arm" being absent in VmlR (*SI Appendix*, Fig. S2 *D–F*). NBD1 of VmlR also establishes interactions with H68 of the 23S rRNA as well as ribosomal protein bL33 (Fig. 2 *A* and *B*). The ARD, linking NBD1 and NBD2, comprises two long α-helices that span from the E site across the interface of the LSU inserting the ARD loop into the PTC (Fig. 2 *A* and *B*). Helix α2 of the ARD runs parallel to H74-H75 and forms multiple contacts with the backbone of nucleotides within these helices, whereas helix α1 interacts predominantly with the acceptor arm of the P-site tRNA (Fig. 2*A*). The elbow region of the P-site tRNA is contacted by NBD2, which establishes additional interactions with ribosomal protein uL5 of the LSU (Fig. 2 *A* and *B*) and h41-42 of the 16S rRNA located within the head of the SSU (Fig. 2*C*). The CTE of VmlR, which has no equivalent in EttA, extends from NBD2 where a short linker guides the CTE between a cleft created by ribosomal proteins uS7 and uS11 on the SSU head and positions the two CTE α-helices into the

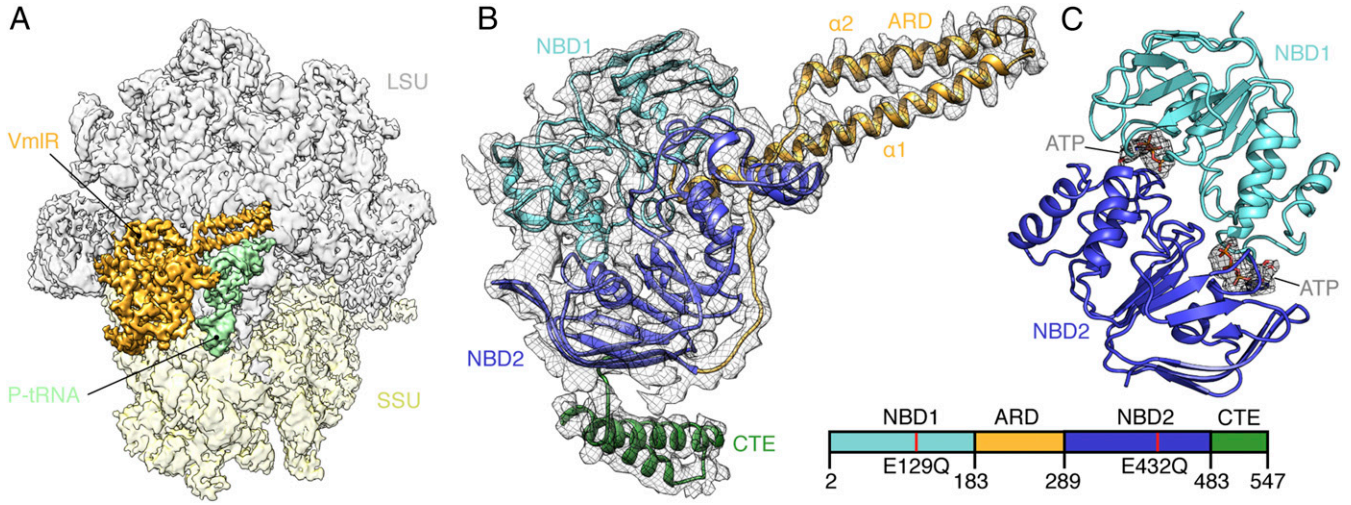

Fig. 1. Structure of VmlR–ribosome complex. (*A*) Cryo-EM map with isolated densities for VmlR (orange), P/V-tRNA (pale green), small subunit (SSU, yellow), and large subunit (LSU, gray). (*B*) Electron density (gray mesh) with molecular model for VmlR, colored according to domains as represented in the schematic (*Bottom Right*): nucleotide binding domain 1 (NBD1, cyan), antibiotic-resistance domain (ARD, orange), nucleotide binding domain 2 (NBD2, blue), and C-terminal extension (CTE, green). (*C*) Molecular model for NBD1 (cyan) and NBD2 (blue) of VmlR with isolated electron density (gray mesh) for the modeled ATP nucleotides (sticks).

Shine–Dalgarno (SD)–anti-SD cavity located on the SSU platform (Fig. 2*C*). This interaction is likely to be important for VmlR function since a VmlR variant lacking the CTE loses its ability to confer antibiotic resistance (*SI Appendix*, Fig. S4 *A–D*), as observed previously for VgaA (9).

VmlR Stabilizes a Noncanonical P/V-tRNA Conformation. Binding of VmlR to the ribosome and accommodation of the ARD at the PTC of the LSU requires the P-site tRNA to be displaced from its canonical position and adopt a noncanonical state, which we term the P/V-tRNA (Fig. 3*A*). The ARD of VmlR is 27 amino acids longer than the equivalent region in EttA (Fig. 3 *A–C*), explaining why binding of EttA does not affect the conformation of the P-site tRNA, nor encroach on the PTC (Fig. 3*B*). Compared with the canonical P-site tRNA position, the elbow region of the P/V-tRNA is shifted by ∼10 Å away from the PTC toward the E site and is likely to be stabilized via interactions with the NBD2 of VmlR (Fig. 3*C*). As a consequence, the CCA end of the P/V-tRNA is redirected by 37 Å into the A site, where it overlaps with the binding site of the acceptor arm of a canonical A-site tRNA, but not with an A/T-tRNA state (Fig. 3*D*). This suggests that the VmlR-stabilized P/V-tRNA would allow delivery of aminoacyl-tRNA to the ribosome by EF-Tu but prevent the subsequent accommodation at the A site of the PTC. It should be noted that the density for the CCA end of the P/V-tRNA was poorly resolved and the nascent chain was not observed (*SI Appendix*, Fig. S5*A*), indicative of high flexibility and consistent with local resolution calculations (*SI Appendix*, Fig. S5*B*). Although we cannot exclude that the nascent chain was hydrolyzed by VmlR, we do not believe this is likely since the

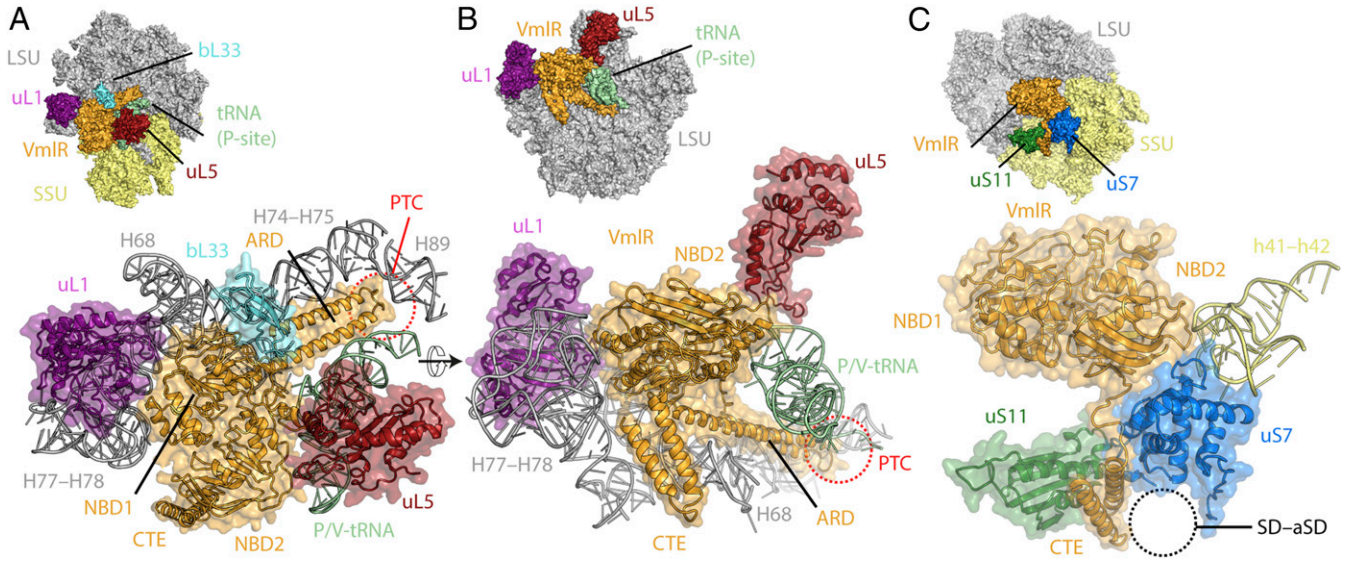

Fig. 2. Interaction of VmlR with the ribosome. (*A–C*) *Inset* and zoom showing VmlR (orange) interaction P/V-tRNA (green) and components of the large subunit (LSU, gray); 23S rRNA helices H68, H74-H75; and H89 (gray) and ribosomal proteins uL1 (magenta), uL5 (red), and bL33 (cyan) (*A* and *B*) and components of the small subunit (SSU, yellow), including 16S rRNA helices h41-42 and ribosomal proteins uS7 (blue) and uS11 (green) (*C*).

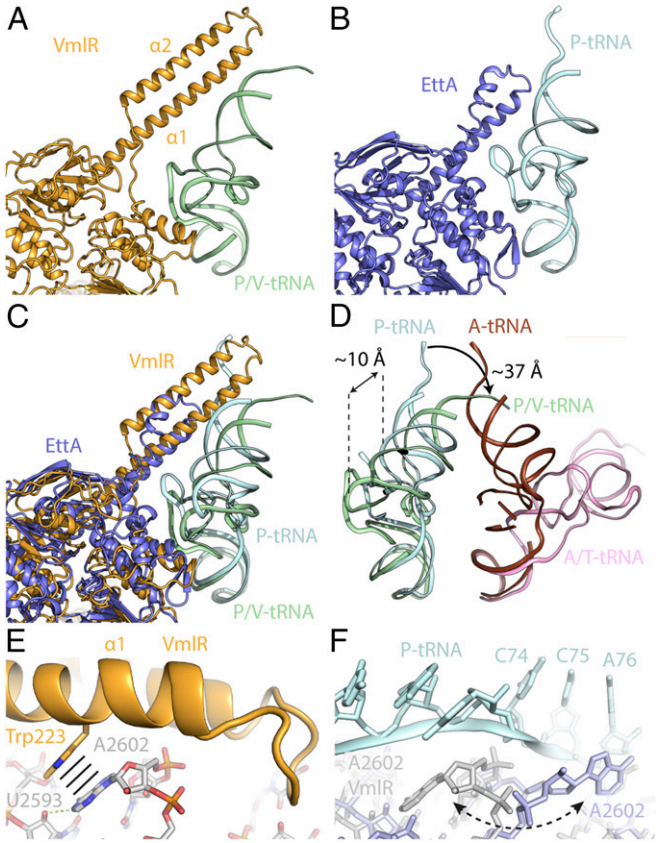

Fig. 3. Comparison of VmlR and EttA on the ribosome. (*A–C*) Relative position of VmlR (orange) and P/V-tRNA (green) (*A*), EttA (blue, PDB ID code 3J5S) (11) and P-tRNA (cyan) (*B*), and superimposition of *A* and *B* (*C*). (*D*) Comparison of P/V-tRNA (green), P-tRNA (cyan), A-tRNA (brown) (39), and A/T-tRNA (pink, PDB ID code 4V5G) (40). (*E*) Stacking interaction (indicated by black lines) of Trp223 of VmlR (orange) with 23S rRNA nucleotide A2602 (gray), which forms hydrogen bonds (dashed lines) with U2593. (*F*) Conformation of VmlR bound conformation of A2602 (gray) compared with the A2602 (slate) conformation in the pretranslocation state conformation (39) with P-tRNA (cyan) and A-tRNA (data not shown).

related VgaA has no detectable peptidyl-tRNA hydrolysis activity (4).

By contrast, the canonical P-site tRNA was well-resolved in the cryo-EM map of the P-tRNA-SRC and the nascent chain could be visualized extending down the ribosomal tunnel toward the telithromycin-binding site (*SI Appendix*, Fig. S5 *E* and *F*). Therefore, binding of VmlR to the ribosome can disengage the P-site tRNA from the PTC despite the presence of the oligopeptidyl-tRNA. Compared with the P-tRNA-SRC, binding of VmlR induces a 3.4° rotation of the SSU body and 4.1° swivel of the SSU head (*SI Appendix*, Fig. S5 *G* and *H*), which may also contribute to destabilizing the P-site tRNA. Displacement of the P-site tRNA from the PTC by the ARD of VmlR leads to a rearrangement in 23S rRNA nucleotide A2602 (*E. coli* numbering is used for rRNA nucleotides) (Fig. 3 *E* and *F*). In the VmlR-SRC, the nucleobase of A2602 stacks upon Trp223 within helix α1 of the ARD of VmlR and forms potential hydrogen bond interactions with U2593 (Fig. 3*E*). By contrast, the VmlR position of A2602 is flipped by 180° compared with the canonical A2602 that interacts with the CCA end of the P-site tRNA (Fig. 3*F*). Therefore, in addition to stabilizing VmlR on the ribosome, flipping of A2602 may also be necessary to clear the way for the transition from the P to the P/V-tRNA state.

VmlR and Resistance to PTC-Targeting Antibiotics. At the PTC, the binding position of helix α1 of the ARD of VmlR overlaps that of the CCA end of a P-site tRNA, whereas the ARD loop and specifically Phe237 extends into the A-site pocket where the aminoacyl moiety of the A-site tRNA normally resides (Fig. 4 *A* and *B*). The A-site pocket is also the binding site of PTC-targeting antibiotics, such as VgM, Lnc, Tia, Cam, and Lnz, whereas S_B antibiotics, such as VgS, and macrolides, such as Ery, bind deeper within the ribosomal tunnel (Fig. 4 *B–D*). While VmlR has been shown to confer resistance to VgM and Lnc, but not to VgS or the macrolides Ery, oleandomycin, and spiramycin (18), the effect on other PTC-targeting antibiotics remains unknown. To test this, we monitored growth of a wild-type (WT) *B. subtilis* strain containing VmlR as well as a *B. subtilis* strain where the *vmlR* gene was inactivated (Δ*vmlR*), in the presence of increasing concentrations of the relevant antibiotics. Growth was also monitored for a Δ*vmlR* strain that was complemented by inserting the *vmlR* gene into the *thrC* locus under the control of an IPTG-inducible promoter. In agreement with previous findings (18), VmlR conferred resistance to VgM and Lnc, but not to Ery (Fig. 4*E* and *SI Appendix*, Fig. S4 *A–C*). In addition, we could also demonstrate that VmlR conferred resistance to Tia, as expected based on the steric overlap between Phe237 of VmlR and the drug, but surprisingly not to Cam or Lnz, which also sterically overlap with VmlR (Fig. 4*E* and *SI Appendix*, Fig. S4 *C–E*).

This observation, coupled with the incomplete conservation of Phe237 (*SI Appendix*, Fig. S1), led us to generate VmlR variants where Phe237 was mutated to Ala (VmlR-F237A) or Val (VmlR-F237V). Growth experiments revealed that the VmlR-F237V retained a WT-like activity profile, conferring resistance to VgM, Lnc, and Tia, but not Ery, Cam, and Lnz (Fig. 4*E* and *SI Appendix*, Fig. S6). By contrast, the VmlR-F237A variant displayed altered specificity, conferring resistance to Lnc and Tia, but not to VgM (Fig. 4*E* and *SI Appendix*, Fig. S6). The retention of resistance activity of the VmlR-F237V variant suggested that VmlR does not employ direct steric interference to dislodge the drug from the binding site at the PTC, but rather an indirect allosteric mechanism. This prompted us to analyze whether the binding of VmlR induced any specific conformational changes within PTC nucleotides that could mediate dissociation of antibiotics from the ribosome. Comparing the PTC conformation in the VmlR-SRC with structures of ribosomes bound with VgM (24), Lnc (25), and Tia (26) revealed the most significant difference for U2585, which is stacked upon by Tyr240 of VmlR, thereby preventing other conformations being adopted that interact with the drugs (Fig. 4 *F–H* and *SI Appendix*, Fig. S7 *F–I*). In addition, shifted conformations were also observed for U2506 and A2062 that may be influenced indirectly by VmlR binding (Fig. 4 *F–H* and *SI Appendix*, Fig. S7 *F–K*).

Discussion

Together with the available literature and the insights gained from the VmlR-EQ_2-SRC structure, we present a model for the mechanism of action of VmlR (Fig. 5) and discuss how it relates to other ARE-ABCF proteins. First, our structure revealed that VmlR recognizes and binds to antibiotic-stalled ribosomes with vacant E sites (Fig. 5 *A* and *B*). We envisage two main scenarios when this can occur during translation, namely, directly following initiation when the E site is free and only an initiator fMet-tRNA is bound in the P site, or subsequent to E-tRNA release from a posttranslocation state during elongation (27). Although a pretranslocational state also has a free E site, we do not believe this is a substrate for VmlR since the relevant PTC-targeting antibiotics prevent A-site tRNA binding and, thereby, block the pretranslocation state from forming. The VmlR-EQ_2-SRC structure suggests that VmlR binds to antibiotic-stalled ribosomes in the ATP conformation with the NBDs adopting a closed conformation (Fig. 5*B*). Binding of VmlR, which is facilitated by important CTE–30S interactions, induces a slight rotation of the SSU relative to the LSU and disengages the P-site tRNA from the PTC, leading to stabilization of a noncanonical P/V-tRNA state (Fig. 5*B*). The VmlR-EQ_2-SRC structure

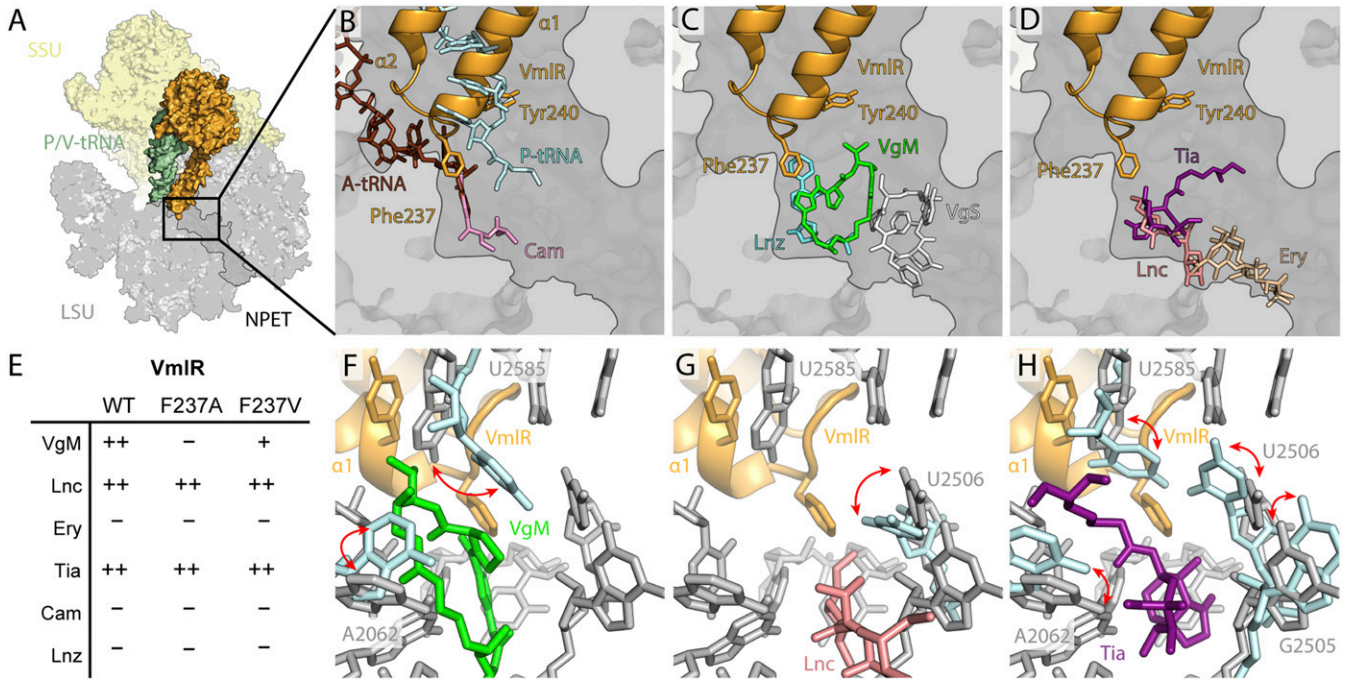

Fig. 4. Interaction of VmlR at the peptidyltransferase center. Overview of VmlR (orange) and P/V-tRNA (green) on the ribosome (SSU, yellow; LSU, gray) (*A*) with transverse section of the LSU to reveal the nascent polypeptide exit tunnel (NPET) with VmlR (orange) superimposed (*B–D*) against A-site tRNA (brown) and P-site tRNA (cyan) from a pretranslocation state (39) and chloramphenicol (Cam, pink, PDB ID code 4V7U) (41) (*B*); virginiamycin M (VgM, green) and S (VgS, white) (PDB ID code 1YIT) (24) and linezolid (Lnz, cyan, PDB ID code 3DLL) (42) (*C*); lincomycin (Lnc, salmon, PDB ID code 5HKV) (25), tiamulin (Tia, purple, PDB ID code 1XBP) (26), and erythromycin (Ery, tan, PDB ID code 4V7U) (41) (*D*). (*E*) Summary of antibiotic resistance conferred by WT VmlR as well as VmlR variants F237A and F237V complementing a Δ*vmlR* strain of *B. subtilis* (see also *SI Appendix*, Fig. S6 *A–F*). (*F–H*) The conformation of selected 23S rRNA nucleotides (gray sticks) at the PTC in the presence of VmlR (orange) superimposed with with different nucleotide (cyan) conformations (indicated by red arrows) when virginiamycin M (VgM, green, PDB ID code 1YIT) (24) (*F*), lincomycin (Lnc, pink, PDB ID code 5HKV) (25) (*G*), and tiamulin (Tia, purple, PDB ID code 1XBP) (26) (*H*) are bound to the ribosome.

revealed that VmlR could even disengage short oligopeptidyl-tRNAs from the PTC, although it remains unclear whether longer peptidyl-tRNA will be refractory to the action of VmlR or other ARE-ABCFs. By inducing a P/V-tRNA state, the ARD of VmlR can access the PTC of the ribosome where it indirectly dislodges the PTC-targeting antibiotics from their binding sites (Fig. 5*B*). This presumably occurs because VmlR induces allosteric conformational changes within PTC nucleotides that comprise the drug-binding site; however, the transition of the P-tRNA to the P/V-tRNA may also contribute to drug dissociation. Surprisingly, our results suggest that VmlR can promote dissociation of some PTC inhibitors, such as VgM, Lnc, and Tia, but not others, such as Cam and Lnz. While we also observe some conformational differences between the PTC bond with VmlR or Cam/Lnz (*SI Appendix*, Fig. S7 *J* and *K*), we note that Cam and Lnz display strong nascent chain-dependent stalling (28), which may preclude VmlR from acting on these stalled complexes, but this needs to be investigated further.

Transpeptidation experiments in the presence and absence of VgaA/Lsa and Lnc indicate that ATP hydrolysis is critical for recycling of ARE-ABCFs (4), suggesting that VmlR-ADP is the low-affinity form that dissociates from the ribosome following drug release (Fig. 5*B*). Moreover, since processive transpeptidation reactions require VmlR-ADP release, the observed

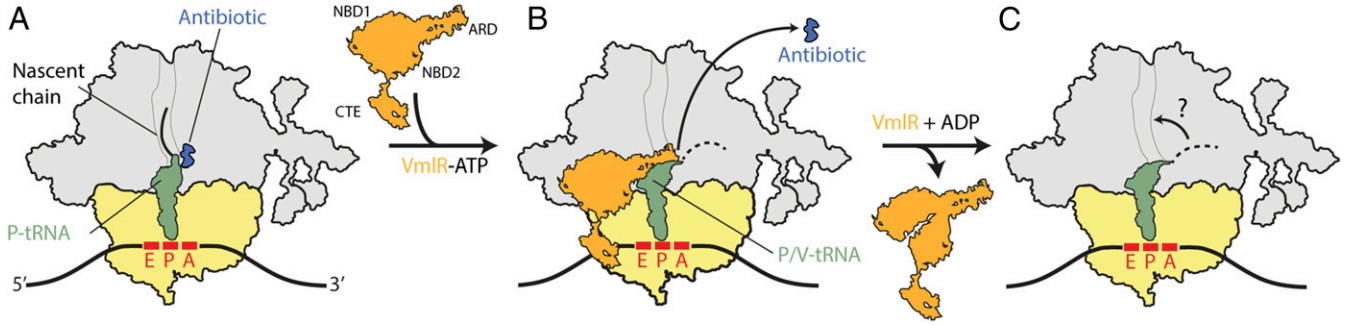

Fig. 5. Model for ribosome protection by VmlR. (*A*) Antibiotic-stalled ribosomes with a peptidyl-tRNA in the P site are recognized by the ABCF ATPase VmlR, which binds to the E site of the ribosome with a closed ATP-bound conformation. (*B*) Binding of VmlR induces a shifted P/V-tRNA conformation in the ribosome allowing the ARD of VmlR to access the peptidyl-transferase center (PTC) and dislodge the drug from its binding. (*C*) Hydrolysis of ATP to ADP leads to dissociation of VmlR from the ribosome, which may allow the peptidyl-tRNA to accommodate back on the ribosome with the nascent chain inserting into the NPET and translation to continue. In *B* and *C*, the dashes line extending from the P/V-tRNA represents a flexible nascent chain.

transpeptidation in the presence of ATP (4) indicates that the P/V-tRNA can reaccommodate at the P site of the PTC (Fig. 5*C*). The transpeptidation experiments were performed with fMet-tRNA (4), thus it is still unclear whether reaccommodation at the PTC can occur with longer peptidyl-tRNAs.

Before submission of this manuscript, a cryo-EM structure was reported of *P. aeruginosa* MsrE in complex with a *T. thermophilus* 70S ribosome bearing a deacylated $tRNA^{fMet}$ in the P site (7). At the time of revision, the cryo-EM map and model were still unavailable, therefore a comparison can only be made based on the publication figures, which are in good overall agreement with the structure and interpretation of the *B. subtilis* VmlR-EQ_2-SRC reported here. The two main differences appear to be that (*i*) MsrE lacks the CTE and therefore also lacks the associated SSU interactions that are available for VmlR, and (*ii*) the ARD loop differs in sequence and length between MsrE and VmlR (*SI Appendix*, Fig. S1) and therefore the interactions at the PTC are likewise distinct. While the ARD loop of MsrE is longer and reaches to the macrolide binding site (7), the VmlR loop is shorter and approaches only the PTC-targeting antibiotics, which is consistent with the respective antibiotic resistance profiles of these proteins.

Materials and Methods

The *B. subtilis* VmlR-EQ_2-SRC was generated by incubating recombinant *B. subtilis* VmlR-EQ_2 protein in the presence of ATP with *B. subtilis* ErmDL-SRC, which were essentially prepared as described (29, 30). Cryo-EM data collection was performed on a Titan Krios 300 kV TEM equipped with a Falcon III DED (FEI). Images of individual ribosome particles were aligned using MotionCor2 (31) and then particles were selected automatically using Gautomatch (https://www.mrc-lmb.cam.ac.uk/kzhang/). All images were processed using RELION 2.1 (20). Final reconstructions were corrected for the modulation transfer function and sharpened by applying a negative B factor estimated by RELION 2.1 (20). The average resolution of reconstructions was determined using the "gold-standard" criterion ($FSC_{0.143}$) (32). ResMap was used for local resolution estimation (33), and the final volumes were locally filtered using SPHIRE (34). Molecular models were fitted and adjusted using Coot (35) and refined in Phenix (36). Model validation was carried out using the MolProbity server (37), and the final model statistics are presented in *SI Appendix*, Table S1. All figures were generated using PyMOL (Schrödinger, LLC) and/or Chimera (38). Further details can be found in the *SI Appendix, Material and Methods*. The cryo-EM maps and models for the VmlR- and P-tRNA-SRC are deposited in the EMDatabank (EMD-0177 and EMD-0176) and RCSB Protein Data Bank (6HA8 and 6HA1), respectively.

ACKNOWLEDGMENTS. We thank Susanne Rieder for expert technical assistance and Seki Takahiro for generating the Δ*vmlR* strain. This research was supported by Deutsche Forschungsgemeinschaft Grants FOR1805 and WI3285/8-1 (to D.N.W.), Swedish Research Council Grants 2013-4680 (to V.H.) and 2015-04746 (to G.C.A.), the Ragnar Söderberg Foundation (V.H.), Carl Tryggers stiftelse CTS 34 (G.C.A.), Jeanssons stiftelse (G.C.A.), and from the Umeå Centre for Microbial Research (UCMR): postdoctoral grant 2017 (to H.T.) and Gender Policy Support 2017 (to G.C.A.). iNEXT, project number 5966, was funded by the Horizon 2020 program of the European Union. Czech Infrastructure for Integrative Structural Biology research infrastructure project LM2015043 funded by Ministry of Education, Youth, and Sports of the Czech Republic is gratefully acknowledged for the financial support of the measurements at the CF Cryo-electron Microscopy and Tomography Central European Institute of Technology, Masaryk University. This article reflects only the author's view, and the European Commission is not responsible for any use that may be made of the information it contains.

1. Wilson DN (2014) Ribosome-targeting antibiotics and bacterial resistance mechanisms. *Nat Rev Microbiol* 12:35–48.
2. Lin J, Zhou D, Steitz TA, Polikanov YS, Gagnon MG (2018) Ribosome-targeting antibiotics: Modes of action, mechanisms of resistance, and implications for drug design. *Annu Rev Biochem* 87:451–478.
3. Sharkey LKR, O'Neill AJ (2018) Antibiotic resistance ABC-F proteins: Bringing target protection into the limelight. *ACS Infect Dis* 4:239–246.
4. Murina V, Kasari M, Hauryliuk V, Atkinson GC (2018) Antibiotic resistance ABCF proteins reset the peptidyl transferase centre of the ribosome to counter translational arrest. *Nucleic Acids Res* 46:3753–3763.
5. Wang Y, et al. (2015) A novel gene, *optrA*, that confers transferable resistance to oxazolidinones and phenicols and its presence in *Enterococcus faecalis* and *Enterococcus faecium* of human and animal origin. *J Antimicrob Chemother* 70:2182–2190.
6. Sharkey LK, Edwards TA, O'Neill AJ (2016) ABC-F proteins mediate antibiotic resistance through ribosomal protection. *MBio* 7:e01975.
7. Su W, et al. (2018) Ribosome protection by antibiotic resistance ATP-binding cassette protein. *Proc Natl Acad Sci USA* 115:5157–5162.
8. Nguyen F, et al. (2014) Tetracycline antibiotics and resistance mechanisms. *Biol Chem* 395:559–575.
9. Jacquet E, et al. (2008) ATP hydrolysis and pristinamycin IIA inhibition of the Staphylococcus aureus Vga(A), a dual ABC protein involved in streptogramin A resistance. *J Biol Chem* 283:25332–25339.
10. Boël G, et al. (2014) The ABC-F protein EttA gates ribosome entry into the translation elongation cycle. *Nat Struct Mol Biol* 21:143–151.
11. Chen B, et al. (2014) EttA regulates translation by binding the ribosomal E site and restricting ribosome-tRNA dynamics. *Nat Struct Mol Biol* 21:152–159.
12. Novotna G, Janata J (2006) A new evolutionary variant of the streptogramin A resistance protein, $Vga(A)_{LC}$, from *Staphylococcus haemolyticus* with shifted substrate specificity towards lincosamides. *Antimicrob Agents Chemother* 50:4070–4076.
13. Lenart J, Vimberg V, Vesela L, Janata J, Balikova Novotna G (2015) Detailed mutational analysis of Vga(A) interdomain linker: Implication for antibiotic resistance specificity and mechanism. *Antimicrob Agents Chemother* 59:1360–1364.
14. Arenz S, et al. (2016) The stringent factor RelA adopts an open conformation on the ribosome to stimulate ppGpp synthesis. *Nucleic Acids Res* 44:6471–6481.
15. Arenz S, Nguyen F, Beckmann R, Wilson DN (2015) Cryo-EM structure of the tetracycline resistance protein TetM in complex with a translating ribosome at 3.9-Å resolution. *Proc Natl Acad Sci USA* 112:5401–5406.
16. Sothiselvam S, et al. (2014) Macrolide antibiotics allosterically predispose the ribosome for translation arrest. *Proc Natl Acad Sci USA* 111:9804–9809.
17. Chiba S, et al. (2011) Recruitment of a species-specific translational arrest module to monitor different cellular processes. *Proc Natl Acad Sci USA* 108:6073–6078.
18. Ohki R, Tateno K, Takizawa T, Aiso T, Murata M (2005) Transcriptional termination control of a novel ABC transporter gene involved in antibiotic resistance in *Bacillus subtilis*. *J Bacteriol* 187:5946–5954.
19. Dönhöfer A, et al. (2012) Structural basis for TetM-mediated tetracycline resistance. *Proc Natl Acad Sci USA* 109:16900–16905.
20. Kimanius D, Forsberg BO, Scheres SH, Lindahl E (2016) Accelerated cryo-EM structure determination with parallelisation using GPUs in RELION-2. *eLife* 5:e18722.
21. Sohmen D, et al. (2015) Structure of the *Bacillus subtilis* 70S ribosome reveals the basis for species-specific stalling. *Nat Commun* 6:6941.
22. Johnson ZL, Chen J (2018) ATP binding enables substrate release from multidrug resistance protein 1. *Cell* 172:81–89.e10.
23. Barthelme D, et al. (2011) Ribosome recycling depends on a mechanistic link between the FeS cluster domain and a conformational switch of the twin-ATPase ABCE1. *Proc Natl Acad Sci USA* 108:3228–3233.
24. Tu D, Blaha G, Moore PB, Steitz TA (2005) Structures of MLS_BK antibiotics bound to mutated large ribosomal subunits provide a structural explanation for resistance. *Cell* 121:257–270.
25. Matzov D, et al. (2017) Structural insights of lincosamides targeting the ribosome of *Staphylococcus aureus*. *Nucleic Acids Res* 45:10284–10292.
26. Schlünzen F, Pyetan E, Fucini P, Yonath A, Harms JM (2004) Inhibition of peptide bond formation by pleuromutilins: The structure of the 50S ribosomal subunit from *Deinococcus radiodurans* in complex with tiamulin. *Mol Microbiol* 54:1287–1294.
27. Choi J, Puglisi JD (2017) Three tRNAs on the ribosome slow translation elongation. *Proc Natl Acad Sci USA* 114:13691–13696.
28. Marks J, et al. (2016) Context-specific inhibition of translation by ribosomal antibiotics targeting the peptidyl transferase center. *Proc Natl Acad Sci USA* 113:12150–12155.
29. Arenz S, et al. (2014) Drug sensing by the ribosome induces translational arrest via active site perturbation. *Mol Cell* 56:446–452.
30. Arenz S, et al. (2014) Molecular basis for erythromycin-dependent ribosome stalling during translation of the ErmBL leader peptide. *Nat Commun* 5:3501.
31. Zheng SQ, et al. (2017) MotionCor2: Anisotropic correction of beam-induced motion for improved cryo-electron microscopy. *Nat Methods* 14:331–332.
32. Scheres SH, Chen S (2012) Prevention of overfitting in cryo-EM structure determination. *Nat Methods* 9:853–854.
33. Kucukelbir A, Sigworth FJ, Tagare HD (2014) Quantifying the local resolution of cryo-EM density maps. *Nat Methods* 11:63–65.
34. Moriya T, et al. (2017) High-resolution single particle analysis from electron cryomicroscopy images using SPHIRE. *J Vis Exp* e55448.
35. Emsley P, Cowtan K (2004) Coot: Model-building tools for molecular graphics. *Acta Crystallogr D Biol Crystallogr* 60:2126–2132.
36. Adams PD, et al. (2010) PHENIX: A comprehensive Python-based system for macromolecular structure solution. *Acta Crystallogr D Biol Crystallogr* 66:213–221.
37. Chen VB, et al. (2010) MolProbity: All-atom structure validation for macromolecular crystallography. *Acta Crystallogr D Biol Crystallogr* 66:12–21.
38. Pettersen EF, et al. (2004) UCSF Chimera–A visualization system for exploratory research and analysis. *J Comput Chem* 25:1605–1612.
39. Polikanov YS, Steitz TA, Innis CA (2014) A proton wire to couple aminoacyl-tRNA accommodation and peptide-bond formation on the ribosome. *Nat Struct Mol Biol* 21:787–793.
40. Schmeing TM, et al. (2009) The crystal structure of the ribosome bound to EF-Tu and aminoacyl-tRNA. *Science* 326:688–694.
41. Dunkle JA, Xiong L, Mankin AS, Cate JH (2010) Structures of the *Escherichia coli* ribosome with antibiotics bound near the peptidyl transferase center explain spectra of drug action. *Proc Natl Acad Sci USA* 107:17152–17157.
42. Wilson DN, et al. (2008) The oxazolidinone antibiotics perturb the ribosomal peptidyl-transferase center and effect tRNA positioning. *Proc Natl Acad Sci USA* 105:13339–13344.